
Taylor & Francis
Taylor & Francis Group

International Journal of Forest Engineering

ISSN: 1494-2119 (Print) 1913-2220 (Online) Journal homepage: www.tandfonline.com/journals/tife20

# Toward a digital twin of forest roads – road weather stations for monitoring road condition and trafficability in Eastern Finland

Kari Väätäinen, Joel Kostensalo, Perttu Anttila, Matti Savinainen, Tomi Kaakkurivaara, Jonne Pohjankukka, Ville Lumberg, Jari Ala-Ilomäki, Juha Laitila, Harri Lindeman, Eugene Lopatin & Lauri Sikanen

**To cite this article:** Kari Väätäinen, Joel Kostensalo, Perttu Anttila, Matti Savinainen, Tomi Kaakkurivaara, Jonne Pohjankukka, Ville Lumberg, Jari Ala-Ilomäki, Juha Laitila, Harri Lindeman, Eugene Lopatin & Lauri Sikanen (29 Jul 2025): Toward a digital twin of forest roads – road weather stations for monitoring road condition and trafficability in Eastern Finland, International Journal of Forest Engineering, DOI: 10.1080/14942119.2025.2533086

**To link to this article:** https://doi.org/10.1080/14942119.2025.2533086



Published online: 29 Jul 2025.

INTERNATIONAL JOURNAL OF FOREST ENGINEERING
https://doi.org/10.1080/14942119.2025.2533086

Taylor & Francis
Taylor & Francis Group



# Toward a digital twin of forest roads – road weather stations for monitoring road condition and trafficability in Eastern Finland

Kari Väätäinen[a], Joel Kostensalo[b], Perttu Anttila[a], Matti Savinainen[c], Tomi Kaakkurivaara[d], Jonne Pohjankukka[b], Ville Lumberg[c], Jari Ala-Ilomäki[a,b], Juha Laitila[a], Harri Lindeman[a], Eugene Lopatin[e], and Lauri Sikanen[a]

[a]Production Systems, Natural Resources Institute Finland (Luke), Joensuu, Finland; [b]Natural Resources, Natural Resources Institute Finland (Luke), Helsinki, Finland; [c]Research Infrastructure Services, Natural Resources Institute Finland (Luke), Tampere, Finland; [d]Faculty of Forestry, Department of Forest Engineering, Kasetsart University, Bangkok, Thailand; [e]Bioeconomy and Environment, Natural Resources Institute Finland (Luke), Tampere, Finland

**ABSTRACT**

Forest roads are crucial for forest management, wood supply, recreation, and wildfire mitigation. However, adverse weather conditions in spring and autumn can weaken these roads, leading to damage and traffic disruptions. This study developed components for a digital twin of forest roads in Eastern Finland, with a focus on weather and moisture monitoring, road structure, traffic monitoring, and their impact on road bearing capacity. Sensors and weather stations reliably monitored road conditions, achieving 99.98% and 100% uptime over a year. Traffic on forest roads was monitored using pressure sensors and game camera images, with a neural network classifying traffic types with 97% accuracy. A light falling weight deflectometer indicated that road bearing capacity during critical periods could decrease to 10–20% of its maximum, underscoring the necessity for reliable real-time solutions to alert road users about road trafficability.

**ARTICLE HISTORY**
Received 10 February 2025
Accepted 27 June 2025

**KEYWORDS**
Bearing capacity; light falling weight deflectometer; neural network; sensor data; timber truck; soil type

## Introduction

Forest roads are a critical component of the forest industry's logistics system. They are essential for sustainable and efficient forest management and wood supply, particularly for timber harvesting, transport activities, and silvicultural operations. Additionally, forest roads play a significant role in recreation and wildfire mitigation. The combined length of gravel-paved roads in Finland is approximately 350,000 km, with forest roads accounting for about 157,000 km (Greis et al. 2019). According to Kulju et al. (2023), the total forest area in Finland is 20.4 million hectares, resulting in an average of 7.7 m of forest road per hectare of forest.

The use and maintenance of forest roads are increasingly challenged by climate change. Historically, winter conditions were more predictable, but recent trends show rising temperatures in late autumn and spring, and shorter winters with ground frost (Lehtonen et al. 2019). Simulations by Ruosteenoja and Jylhä (2021) projected an average increase of 3–4°C in winter temperatures and a 2°C rise in summer temperatures for the period 2040–2069 compared to 1981–2010.

Efficiency targets for reducing costs and emissions have necessitated the use of larger trucks for timber transport. In Finland, the maximum allowed weight of timber trucks was increased from 60 to 76 tonnes in 2013 (FinLex 2013). However, the timing of heavy timber transports is crucial, as heavier trucks are more likely to cause significant damage to roads under adverse weather conditions. If the technical structure of the road is compromised due to overloading relative to its current bearing capacity, transport will be halted, and the necessary reconstruction of the road will be both expensive and time-consuming (Vuorimies et al. 2015; Kaakkurivaara and Korpunen 2017). Shorter winters, characterized by shorter periods of ground frost and more extreme variations in precipitation, necessitate greater anticipation of road conditions. The narrowing operational window for timber transport requires more real-time data for decision-making. Additionally, the deterioration of forest roads continues due to insufficient rehabilitation and maintenance activities (Solonen et al. 2023).

Forest roads are primarily designed and constructed for forestry needs, with a low volume of traffic. The majority of forest roads in Finland were established between the 1960s and 1990s (Kaakkurivaara et al. 2015), when the gross vehicle weight of timber trucks was lower, and transports were more frequently timed during periods of frozen ground or hard soils in non-frozen seasons. Most forest roads have been built using materials available at the construction site, sometimes with inadequate and improper materials for the road structure (i.e. base and subbase course) (Kaakkurivaara et al. 2015). The insufficient bearing capacity of a road is often caused by inadequate (i.e. too thin) superstructure layers, the mixing of layers with frost-susceptible subgrade soil, and inadequate drainage of the road structure (Hämäläinen 2012; Greis et al. 2019).

In Finland, there are classification instructions for constructing and rehabilitating forest roads based on different subgrades and estimated traffic volumes to achieve the targeted

**CONTACT** Kari Väätäinen kari.vaatainen@luke.fi Natural Resources Institute Finland (Luke), Yliopistokatu 6, 80100 Joensuu, Finland

minimum bearing capacity, measured by the modulus of elasticity (E-modulus) (Metsätieohjeisto 2001; Strandström 2017). Common issues with gravel roads include rutting due to low bearing capacity, dust, potholes, corrugation, inadequate drainage capacity, disintegration of gravel, loose gravel, and frost damage (Alzubaidi and Magnusson 2002; Saarenketo and Aho 2005). The challenges in timber harvesting and logistics arise during seasons with poor road conditions and on roads that lack adequate year-round trafficability for heavy vehicles.

The term "digital twin" (DT) was first introduced by Grieves in 2003 as a "digital equivalent to a physical product" (Jones et al. 2020). NASA's Apollo space program was the first to use the "twin" concept by having a physical twin of a space vehicle to mirror, simulate, and predict the conditions of the vehicle in space (Liu et al. 2021). Over the past 20 years, digital twins have been widely used for industrial, servicing, and academic purposes across various applications and technologies (Jones et al. 2020; Liu et al. 2021). The term "digital twin" and its use cases have evolved significantly. The most common description of a DT is a digital model (virtual representation) of an intended or actual real-world physical product, system, or process (a physical twin) that serves as an effectively indistinguishable digital counterpart for practical purposes such as simulation, integration, testing, monitoring, and maintenance (Boschert and Rosen 2016; Jones et al. 2020).

Continuous, often big-data-driven monitoring using multiple measurement and monitoring methods of the target object, system, or process is essential for detailed, high-fidelity modeling of the physical twin. The quality and validity of monitoring data play a decisive role in the development of a DT. In industrial and practical use cases, DTs typically support decision-making by presenting the system's status and generating real-time predictions (Digital Twin Consortium 2025).

Most DT frameworks related to roads have been designed for high-volume roads to optimize construction and maintenance and predict road conditions (Chen et al. 2022; Steyn and Broekman 2022; Consilvio et al. 2023). A few frameworks have been developed for planning road networks in urban (Jiang et al. 2022) and agricultural areas (Machl et al. 2019). Meža et al. (2021) presented a pilot study to establish a DT for a road construction project, targeting the use of secondary road materials in road construction. This study utilized multisource road sensor data, including temperature, vertical deformation, soil moisture, asphalt strain, and pressure sensors. Chen et al. (2022) concluded in their literature review that to predict road performance and condition with a DT, monitoring data should include: i) existing performance index, ii) existing distress condition, iii) road materials, iv) road structure, v) climate, and vi) traffic.

Monitoring weather conditions (e.g. temperature, moisture content, frost, thawing), mechanical properties (e.g. bearing capacity, road deformation), and structure (e.g. road layers, profile, dimensions) of forest roads using sensors and nondestructive measuring devices has been carried out in several studies. These studies include those conducted in Finland (Saarenketo and Aho 2005; Kaakkurivaara 2018), Norway (Fjeld et al. 2022, 2023), and Austria (Holzleitner et al. 2020). The aims of precise monitoring of forest roads are to identify factors contributing to road surface and structure wear and deformation, understand spring thaw and wet season weakening, and find solutions to mitigate road deterioration to maintain roads in a trafficable condition for heavy vehicles (Saarenketo and Aho 2005; Holzleitner et al. 2020; Fjeld et al. 2022; Niskanen et al. 2024).

In a report by Saarenketo and Aho (2005), detailed road structure and condition monitoring with extensive field tests was presented, focusing on studying spring thaw weakening, the factors affecting it, and how roads react to heavy traffic. Percostations were used to measure road water content, the physical state of water, and the mechanical properties from the pavement to the subgrade of the road. Kaakkurivaara (2018) examined portable tools to measure the bearing capacity of different types of forest roads through the seasons to detect attributes affecting trafficability. In Austria, Holzleitner et al. (2020) established a measurement setup for monitoring weather, road conditions, and road trafficability. Data from an automated road station (measuring moisture and temperature of a road at varying depths and ambient weather parameters) and manual measurements of bearing capacity were used to identify and study the impact of weather conditions on the bearing capacity of forest roads.

Fjeld et al. (2022) measured forest roads by assessing bearing capacity, materials in the road structure, volume of heavy traffic, and road deformation to lay a foundation for forecasting the seasonal trafficability of forest roads. Niskanen et al. (2024) used automatic monitoring of road properties to assess the impact of a 84-tonne GVW high-capactity timber truck and other heavy traffic on both paved and gravel roads in Northern Finland across different seasons. The monitoring included road weather parameters from percostations, road pressure and bearing capacity measurements, and counting of heavy traffic. Roadscanners Ltd. introduced the first road monitoring station system (percostation) nearly 25 years ago, which has been used to monitor variations in water content, the physical state of water, and the mechanical properties of the road structure and subsoil during different seasons on both paved and gravel roads in several countries, including Finland, Sweden, and Scotland (Roadscanners 2025).

According to the conclusions of Saarenketo and Aho (2005) and Solonen et al. (2024), more accurate information on the suitability of forest roads for heavy traffic in different weather conditions and seasons would improve the efficiency of forestry operations and timber supply, save road repair costs by limiting heavy traffic on roads with low bearing capacity, and support sustainable road management by conserving depleting gravel materials. Today, the level of technology and digitalization enables the efficient use of large data sets and the creation of digital twins for improved decision-making. However, there are still no implementations for long-term monitoring of the condition, road-weather behavior, and trafficability of low-volume forest roads.

## Aim of the study

In order to investigate the year-round road-weather dynamics and bearing capacity of forest roads, key components for monitoring the trafficability of forest roads and road-weather parameters were designed and implemented. The aim was to demonstrate and validate the feasibility of specific technical

solutions for monitoring forest roads in the context of creating digital twins of forest roads in the future. This paper focuses on the methodology, presenting key results of the monitoring systems setup through several examples.

## Materials and methods

### Establishment of road weather stations

A total of 10 road segments, each approximately 100 m in length, were selected in Eastern Finland (Figure 1). The aim was to acquire segments representative of typical forest road sites on different subsoils and with varying road structures. The following criteria were applied in the selection:

(1) The segments represent different types of forest roads with respect to subsoil, topography, and condition.
(2) The segments are located in the vicinity of the Joensuu research station to enable bearing capacity measurements on short notice when the weather changes
(3) The segments are geographically clustered to ensure cost-efficient measurement of bearing capacity and weather parameters, i.e. groups of two or three nearby segments are formed.
(4) The road owner must be willing to support the project and be interested in using the results.

The primary selection criterion was subsoil type to ensure that roads on different types of soils were included. For the selection, open-source data on superficial deposits in Finland provided by the Geological Survey of Finland (GTK) were used (GTK 2018). The selected segments covered soil types ranging from fine-grained soils (e.g. peat and clay) to coarser soils such as sand and gravel. To ensure the accuracy of the subsoil classification and to determine the road structure, soil samples were collected and analyzed from each segment.

### Road layers and soil types

Core drilling was conducted to define the road structure, road material, and subsoil for each road segment. Soil samples were collected from all road structure layers for detailed laboratory analysis. Core drilling was performed using a van-trailer-based light hammer drilling machine with a drill core head of 10 cm width and 150 cm length. Samples were drilled at a distance of 1 m from each sensor location positioned in the wheel path. A total of 30 drillings were completed.

The drilling depth was 1.2 m or until the core drill could not reach the threshold depth after two attempts (mainly due to encountering a large stone or bedrock). The structure and thickness of road layers were measured to an accuracy of 1 cm. Soil type, grain size distribution, and moisture content were analyzed following the standards 2003, 2013, and 2010.

The layers for all road sections were classified into three main categories: i) wearing and base course, ii) subbase, and iii) subgrade (i.e. subsoil). The wearing and base courses were combined into one layer class based on the sampling results, as it was not possible to separate these layers in most sections.

The depth from the road (wheel path) surface to the transition line of road layers was presented in centimeters, measured with a measuring stick from the undisturbed core soil sample drilled from the road. From the standardized grain-size


Figure 1. Locations of the 10 road segments used in this study.

analysis, the study-specific soil-type classification was derived according to the proportions of the main soil types: stone, gravel, sand, silt, and clay. Soil types with content greater than 10% were expressed in the classification of this study before other soil types with higher concentrations (e.g. "Silty gravelly sand," meaning that 10% < silt < gravel < sand). Additionally, if the soil type included fine-grained soils (clay, silt) or peat exceeding the thresholds of the standard, the susceptibility to freezing was expressed for each sample and layer.

### Automated road weather stations

Nine combined temperature and humidity sensors (2024) were installed in each road segment (Figure 2). The locations were chosen to ensure that the sensor positions varied as much as possible in terms of road topography, visually observed subsoil on the sides of the road, and road condition. The sensors were placed at three different locations along the road at three depths: 20–25 cm, 50–55 cm, and 80–85 cm. The distance between the sensor sets was approximately 20–40 m. The sensors were installed in 35-mm holes drilled into the road at a 45-degree angle, filled with fine sand, and each sensor plate was oriented slightly inclined (10 degrees) with respect to the wheel path (Figure 2).

To validate sensor accuracy for measuring soil moisture content (volumetric water content, VWC), a laboratory test was conducted using three sandboxes mixed with water and one sandbox without water. Three SMT100 sensors were tested in each box for two 15-h test runs. The same fine-grained sieved sand (grain size 0.1–0.6 mm) used in sensor installation on roads was used in the lab tests.

The road sensors were cabled to junction boxes near the measurement points and from the boxes to the datalogger. The power supply for the sensors was connected to the battery and the solar-panel-powered system of the measuring station. All aboveground and underground cabling was installed in flexible 20-mm conduit. All variables were measured every hour, and the measurement data were stored on the datalogger, from where it was transferred to the measurement computer located in Joensuu via a 4 G modem. Additionally, the data were transferred once a day to the network data storage of the Natural Resources Institute Finland. All sensors in the measurement system (SMT100 and WXT530) were SDI-12 bus, so the measured readings were received as serial data.

One weather station unit was installed for each cluster of road segments, positioned approximately 1.5 m above the road surface. Thus, data from one weather station corresponded to 2–3 road stations. Ambient weather parameters measured by the Vaisala W×T530 weather station included wind direction, wind speed, air temperature, relative humidity, barometric pressure, precipitation, and the amount of ice granules.

### Monitoring of bearing capacity

Falling weight deflectometers have been used to estimate the stiffness and bearing capacity of roads by measuring road surface deflection and the E-modulus of forest roads

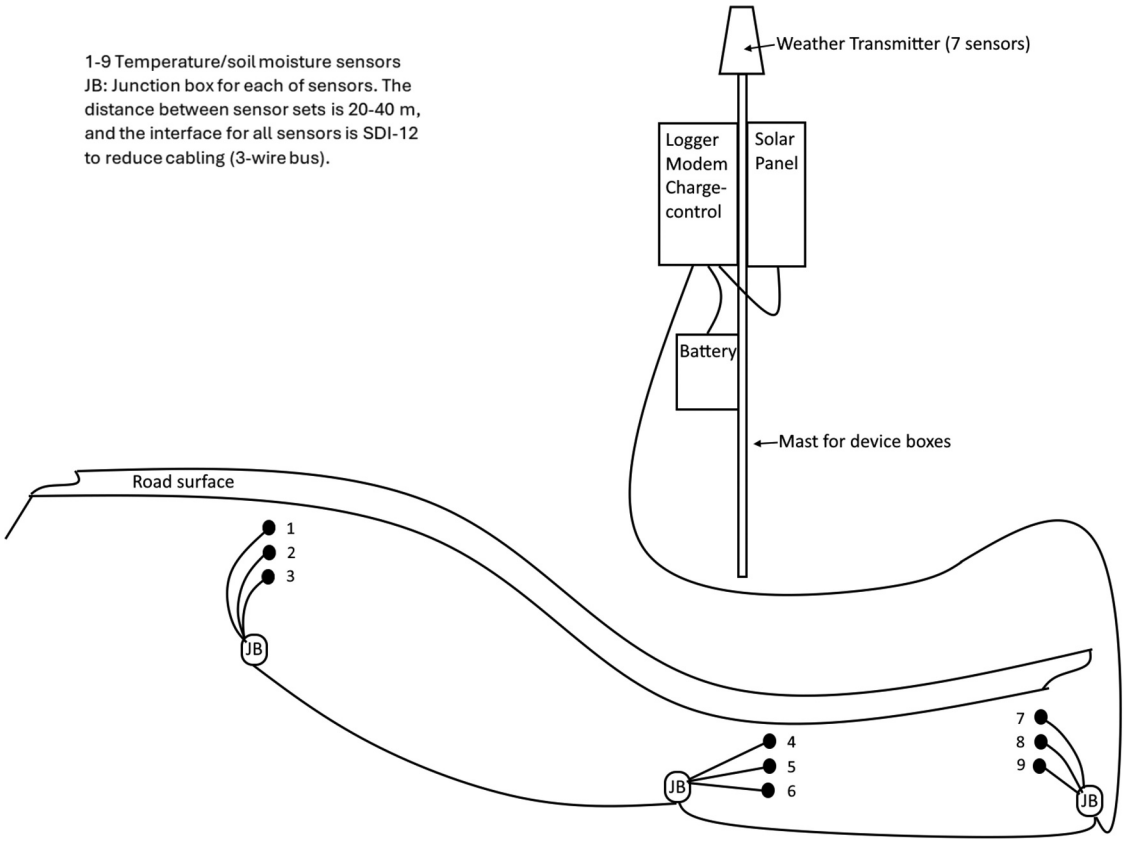


Figure 2. A schematic representation of a road weather station.

(Kaakkurivaara 2018; Fjeld et al. 2023; Karjalainen et al. 2024). The E-modulus, in turn, predicts road trafficability (Kaakkurivaara 2018). In this work, the dynamic deformation modulus (Evd) in MPa was measured using a light falling weight deflectometer (LFWD) Zorn ZFG 3.1 (ZFG 2024). The modulus of elasticity is calculated using the road surface deflection derived from the accelerometer of the bearing plate, according to the Equation (1) (Pidwerbesky 1997a, 1997b; 2021):

$$E_{vd} = 1.5(p * a/\Delta) \quad (1)$$

Where,
$E_{vd}$ = dynamic deformation modulus (MPa)
$\Delta$ = deflection under the load plate
$p$ = vertical pressure of the load plate
a = radius of the load plate

Each measurement consisted of three pre-load falls and three measurement falls, with the result being the average of the latter three. Due to the low bearing capacity of the roads, a 98.1 N drop hammer weight (mass of 10 kg) with an impact load of 7.07 kN and a 30 cm load plate were used. The Evd can be influenced by partial discontinuities within a depth of twice the diameter of the loading plate, giving an influence zone of 60 cm (Kim et al. 2023). Measurements were taken at 20 m intervals, totaling six and seven measurement locations on Road 1 and Road 2, respectively. At each measurement location, a measurement point was located on both wheel paths. Additionally, on Road 2, Evd was measured at the center line of the road.

### Stress test

Rutting of the road segments was measured in stress tests to establish the link between E-modulus values and road trafficability for heavy vehicles, such as a loaded timber truck. Stress tests were conducted on road segment 2 (Road 2) in spring 2022 (17 May 2022) using a loaded timber truck without a trailer. The test truck was a Volvo FH16 (model year 2020) with four axles and an attached self-loader. The total weight of the loaded truck was 39,360 kg, including 17,440 kg of timber. The masses were weighed on a bridge scale at Stora Enso's mill timber reception in Varkaus. The truck's mass was distributed among the axles as follows: 23%, 23%, 31%, and 24% from front to rear (estimated proportions from the truck's own air-suspended axle weighing system). The first two axles had single tires, with the steering axle having 385/65R22.5 tires and the rest 385/55R22.5 tires. The last two axles had twin tires. The distances in centimeters between the steering axle and the following three axles were 225, 510, and 650. Tire pressures were 8.2–8.3 kPa on all tires except the steering axle, which had 9.0 kPa.

Before the stress test, measurement points were marked on the intended left and right wheel paths at 20 m intervals. The initial road surface levels were measured with a laser leveler and a measuring scale bar just before the first truck pass at the predefined measuring points. Additionally, the rut depth caused by vehicle passes was measured after 2, 4, 6, 8, 10, 20, and 30 truck passes over each road section. During the passes, the driving speed was 15 km per hour.

Soil pressure was measured to determine the extent of vehicle-induced pressure reaching deeper layers in the road structure, as increasing moisture content results in softer soil (Söhne 1958). The method could be useful for dimensioning the layers of the road structure. The soil pressure induced by the timber truck was measured using a Bolling probe (Keller et al. 2016) provided by the Bern University of Applied Sciences. The Bolling probe consists of a thin-walled soft silicone hose connected to a pressure transducer via a rigid plastic tube. The hose and tube were inserted into the road structure through drilled holes and filled with water to transmit pressure from the silicone hose to the transducer. The target depths of the pressure-sensing elements in the road structure were 0.2 m, 0.4 m, and 0.6 m. Pressure was measured with digital pressure transducers via an RS 485 serial communication bus to a laptop computer at a frequency of approximately 15 Hz.

### Traffic monitoring with AI-based machine vision

In addition to structure and weather, gravel roads are affected by traffic and maintenance. On one hand, heavy vehicles – and on thawing season even cars – may cause rutting on the roads. On the other hand, maintenance operations such as gravel bedding, surface leveling, and removal of snow cover influence the bearing capacity. Therefore, it would be useful if the type and volume of traffic and maintenance activities on the road segments could be automatically detected.

Machine-vision-based interpretation of photos taken with game cameras could offer a way to provide the necessary information. A total of 1,016 photos were captured from two road segments and used in the analysis (Table 1). The photos were manually labeled into four classes: 1) Cars and vans (466 photos), 2) Heavy vehicle (113), 3) Tractor (56), and 4) Other (362). Furthermore, 19 blurred or ambiguous photos were left out from the analysis. Class 2 included photos of timber truck combinations (both empty and laden), refuse collection vehicles, and snowplow trucks.

A convolutional neural network (CNN) model based on the pre-trained ResNet50 (He et al. 2016) architecture was applied for multi-class image classification. The convolutional layers use fixed ImageNet (Deng et al. 2009) weights as the feature extractor. Custom trainable layers were added on top of the fixed convolution base layer, including 2D

**Table 1.** Traffic data from game camera photos.

| | Camera | |
|---|---|---|
| | Reolink Go 4 G | Burrell S12HD+SMS3 |
| Road number | 3 | 2 |
| Number of photos | 740 | 276 |
| Time period | 16 Sep 2022–19 Jan 2023 | 14 Sep 2022–9 Nov 2022 |

global average pooling and four fully connected (dense) layers with 512, 256, 128, and 64 nodes, each utilizing ReLU activations. Dropout layers with a 50% drop rate were utilized after each dense layer to prevent model overfitting. The final output layer was a dense layer with four units and softmax activation, producing a probability distribution over the target classes. The CNN was trained using the Adam optimizer (Kingma and Ba 2015) with sparse categorical cross-entropy as the loss function. A batch size of 32 was used, and the model was trained for a maximum of 3,000 epochs. The photo dataset was split in a stratified manner into random train (70%), validation (20%), and test (10%) sets. In stratified splitting, the class proportions in the train, validation, and test sets mirror the proportions of the classes in the full dataset, minimizing the risk of biased performance evaluation. Computations were performed using the Keras (Chollet 2015) and TensorFlow (Abadi et al. 2016) libraries.

## Results

### Road structures

According to the soil sample analysis conducted for each road segment and road sensor location, the roads contained a good variation of different soil types (Table 2). For all segments, the average depth of the wearing and base course was 21 cm, ranging from 5 to 45 cm. The average thickness of the subbase was 41 cm, ranging from 15 to 70 cm. The subgrade started at an average depth of 63 cm from the road surface. The depth of

**Table 2.** Soil types in each road segment and road sensor location derived by the soil sample analysis and subsoil types based on superficial deposits reported by the Geological Survey of Finland (GTK) 1:20 000/1:50 000 data. Numbers in brackets indicate the road layers from top to bottom. The frost susceptibility (yes, no) is shown for the road layers. Segment number refers to the map in fig. 1.

| Road segment & sensor location | Wearing and base course (1), depth in cm | Subbase (2), depth in cm | Subgrade (3), start depth in cm | Frost susceptibility (1) | Frost susceptibility (2) | Frost susceptibility (3) | Subsoil type by the GTK data |
|---|---|---|---|---|---|---|---|
| 1.1 | Sandy gravel, −45 | Stony gravel, 45–70 | Peat with wooden layer, 70 | Yes | No | Yes | Carex peat/sand |
| 1.2 | Sandy gravel, −35 | Silty sandy gravel, 35–60 | Peat with wooden layer, 60 | Yes | Yes | Yes | Carex peat/sand |
| 1.3 | Gravelly sand, −37 | Silty sand with humus, 37–50 | Sand, 50 | Yes | Yes | No | Carex peat/sand |
| 2.1 | Gravelly sand, −35 | Silty gravelly sand, 30–75 | Peat with wooden layer, 75 | Yes | Yes | Yes | Carex peat |
| 2.2 | Gravelly sand, −40 | Silty gravelly sand, 40–60 | Peat with wooden layer 60 | Yes | Yes | Yes | Carex peat |
| 2.3 | Gravelly sand, −55 | Silty gravelly sand, 55–84 | Peat with wooden layer, 84 | Yes | Yes | Yes | Carex peat |
| 3.1 | Gravelly sand, −13 | Gravelly sand, 13–73 | Claey silt, 73 | Yes | Yes | Yes | Sandy moraine |
| 3.2 | Gravelly sand, −12 | Gravelly sand, 12–85 | Claey silt, 85 | Yes | Yes | Yes | Sandy moraine |
| 3.3 | Gravelly sand, −17 | Silty sand, 17–35 | Silty gravelly sand, 35 | Yes | Yes | Yes | Sandy moraine |
| 4.1 | Gravelly sand, −20 | Silty clay, 20–90 | Silty clay, 90 | Yes | Yes | Yes | Clay |
| 4.2 | Gravelly sand, −15 | Sandy gravel, 15–38 | Silty clay, 38 | Yes | No | Yes | Clay |
| 4.3 | Gravelly sand, −20 | Sandy gravel, 20–60 | Gravelly silty sand, 60 | Yes | No | Yes | Clay |
| 5.1 | Sandy gravel, −30 | Silty sand, 30–53 | Peat, 53–130 | Yes | Yes | Yes | Sandy moraine |
| 5.2 | Sandy gravel, −10 | Silty sandy gravel, 10–45 | Silty sandy gravel, 45 | Yes | Yes | Yes | Sandy moraine |
| 5.3 | Sandy gravel, −15 | Silty sand, 15–30 | rock/big stone, 30 | Yes | Yes | No | Sandy moraine |
| 6.1 | Sandy gravel, −20 | Gravelly silty sand, 20–75 | Silty peaty sand, 75 | Yes | Yes | Yes | Carex peat/sandy moraine |
| 6.2 | Sandy gravel, −25 | Gravelly silty sand, 25–70 | Silty peaty sand, 70 | Yes | Yes | Yes | Carex peat/sandy moraine |
| 6.3 | Sandy gravel, −8 | Silty sand, 8–35 | Gravelly silty sand, 35 | Yes | Yes | Yes | Carex peat/sandy moraine |
| 7.1 | Gravelly sand, −15 | Sand, 15–80 | Sand, 80 | Yes | No | No | Sand |
| 7.2 | Gravelly sand, −10 | Sand, 10–80 | Sand, 80 | Yes | No | No | Sand |
| 7.3 | Gravelly sand, −15 | Sand, 15–55 | Sandy silty clay, 55 | Yes | No | Yes | Sand |
| 8.1 | Gravelly sand, −5 | Silty sand, 5–50 | Silty sand, 50 | Yes | Yes | Yes | Fine sand |
| 8.2 | Gravelly sand, −23 | Sand, 23–90 | Silty sand, 90 | Yes | No | Yes | Fine sand |
| 8.3 | Gravelly sand, −8 | Silty sand, 8–70 | Silty sand, 70 | Yes | Yes | Yes | Fine sand |
| 9.1 | Sandy gravel, −12 | Gravelly sand, 12–60 | Gravelly sand, 60 | No | Yes | Yes | Gravel |
| 9.2 | Sandy gravel, −23 | Gravelly sand, 23–60 | Gravelly sand, 60 | No | Yes | Yes | Gravel |
| 9.3 | Sandy gravel, −12 | Gravelly sand, 12–55 | Gravelly sand, 55 | No | Yes | Yes | Gravel |
| 10.1 | Sandy gravel, −35 | Stony sand, 35–55 | Silty sandy gravel, 55 | Yes | Yes | Yes | Sandy moraine |
| 10.2 | Sandy gravel, −15 | Fine sand, 15–75 | Silty sandy gravel, 75 | Yes | Yes | Yes | Sandy moraine |
| 10.3 | Sandy gravel, −13 | Stony sand, 13–69 | Silty sandy gravel, 75 | Yes | Yes | Yes | Sandy moraine |

the subgrade transition line ranged from 35 to 90 cm across all sampled road sections. The subsoil type derived from the open GTK data matched the soil sampling results well for the subgrade, with approximately two-thirds of the matches being correct.

### Road weather station data

In method validation, hybrid moisture-temperature sensors provided relatively accurate results for the volumetric water content (VWC) compared to the volume-scaled calculation (Table 3). The estimated accuracy of the VWC in terms of root mean square error (RMSE) was 2.18 percentage points under laboratory conditions.

During the one-year period from 15 October 2021, at 12:00 to 15 October 2022, at 11:00, the logging system for Road 2 functioned without fault, logging sensor information hourly. For the sensor system on Road 2, there were two missed logging events on consecutive days (25 November 2021, at 9:00 and 26 November 2021, at 11:00), meaning the system functioned without problems 99.98% of the year. The weather station data functioned without downtime throughout the year.

The air temperature and rainfall measurements from the weather station, along with the sensor data from the middle of the road segment, are presented in Figure 3. The air temperature measurements appeared reasonable, and the road temperature measurements seemed to be a smoothed-out version of the air temperature, with temperatures staying at or above 0°C during the winter months. The road temperatures remained relatively consistent throughout the year, though the measurements from deeper layers showed less variation, with slightly lower temperatures in the summer and higher temperatures in the winter compared to those closer to the surface.

The pattern of rainfall matched the peaks in moisture well at depths of 0.2 m and 0.5 m. At 0.8 m, there was a little variation over the year. However, the absolute values of the rainfall measurements were inaccurate as the recorded rainfall for the year totaled 1,584 mm, although no rainfall was recorded during the winter months due to the sensor's inability to detect snowfall.

The bearing capacity measurements carried out on Roads 1 and 2 are shown in Figure 4 for the period from 15 October 2021, to 15 October 2022. On both roads, the time evolution of the bearing capacity was quite uniform across all measurement locations. For Road 1, both sides of the road had similar bearing capacities, except at the location 60 m from the starting end, where the left side consistently had a lower

**Table 3.** Results from a validation test of the accuracy of estimating VWC by the truebner SMT100 sensor in laboratory conditions using fine-grained sand with four trials.

| Trial no | Water volume ($dm^3$) | Sand + Water volume ($dm^3$) | VWC (%) | SMT100, VWC (%) (avg) | SMT100, VWC (%) (SD) |
|---|---|---|---|---|---|
| 1 | 0.00 | 3.02 | 0.00 | 0.35 | 0.11 |
| 2 | 0.25 | 3.04 | 8.21 | 4.79 | 0.23 |
| 3 | 0.90 | 3.03 | 29.72 | 27.40 | 0.31 |
| 4 | 1.20 | 3.02 | 39.80 | 38.48 | 0.41 |

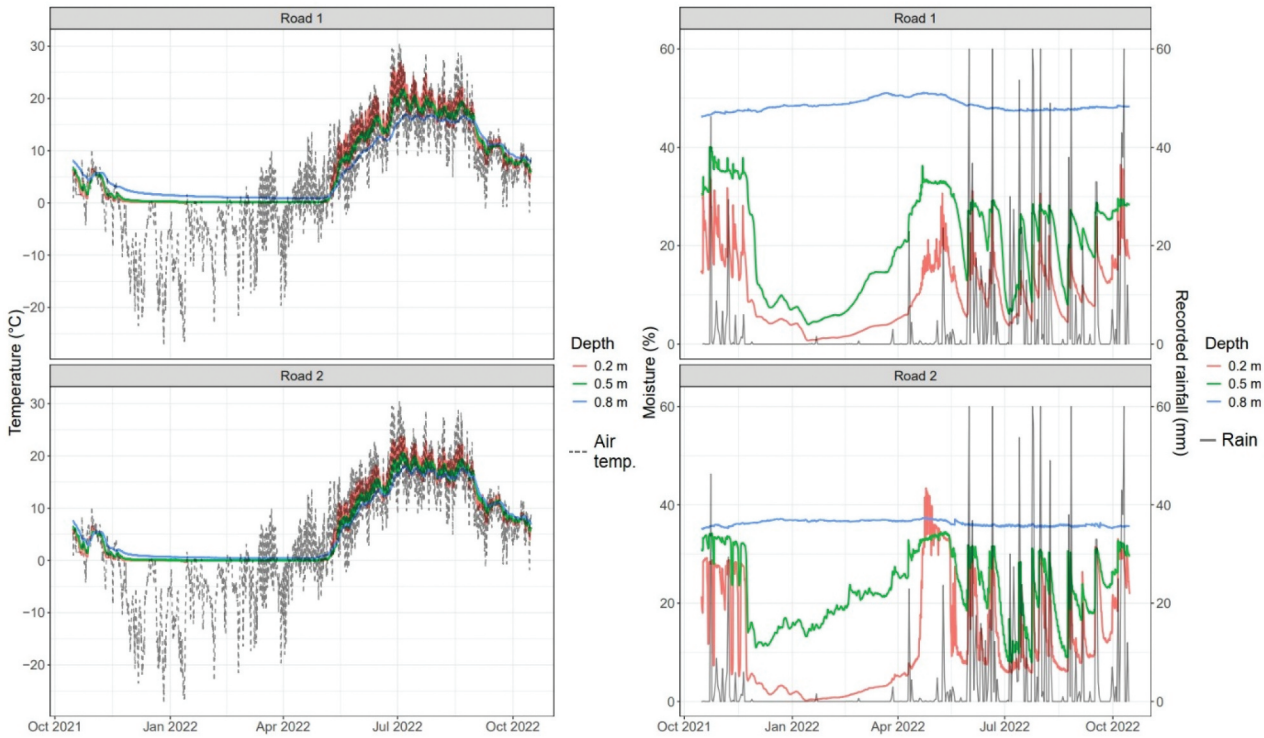


**Figure 3.** Air temperature and rainfall measurements from the weather station and the sensor data from the middle of the road segment over the period 15 October 2021–15 October 2022.

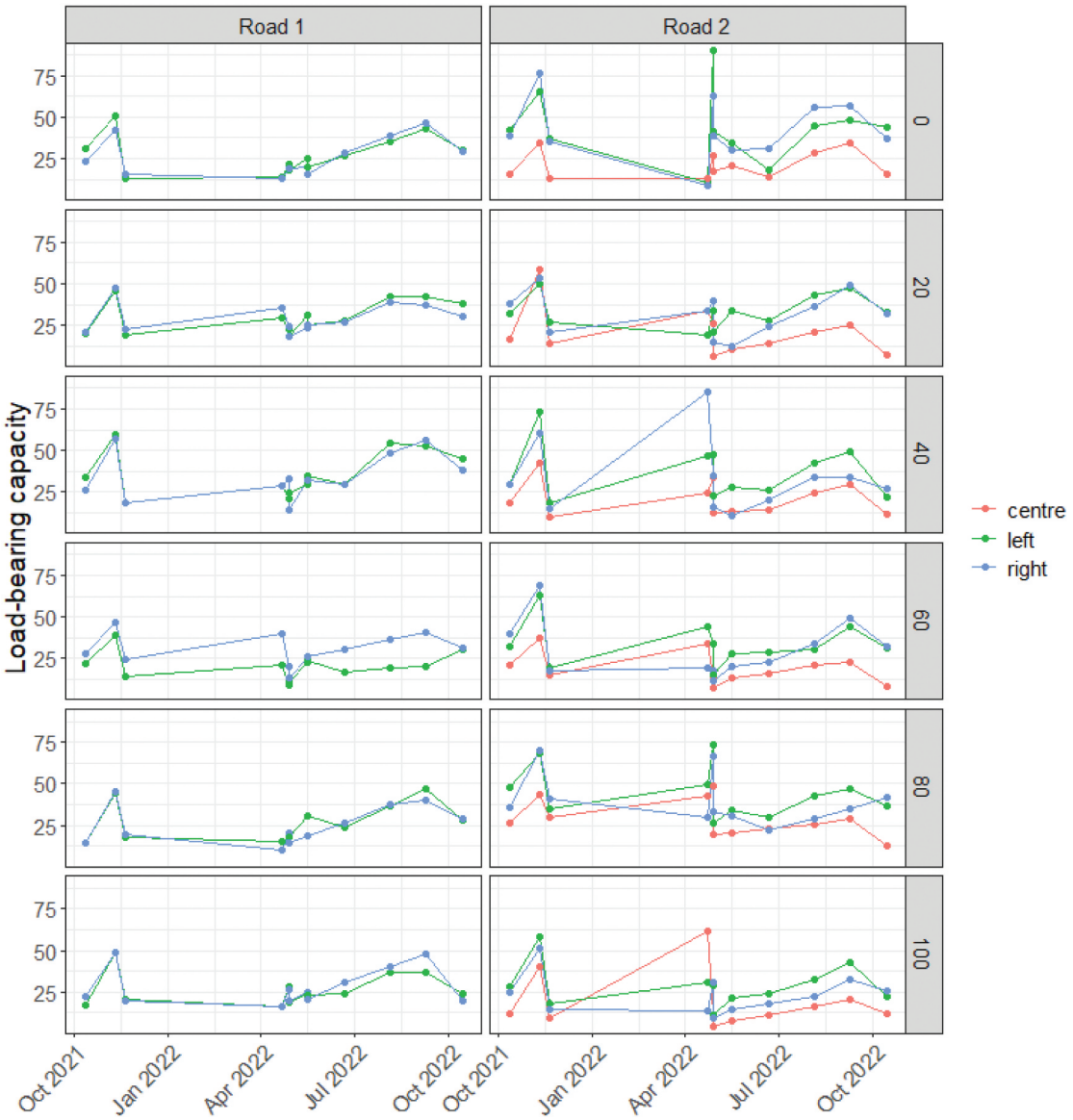


**Figure 4.** Bearing capacity monitoring over the period 15 October 2021–15 October 2022, for road segments 1 (left) and 2 (right). Each subfigure shows the measurements from one location starting from one end of the segment (0) and proceeding in 20 m intervals to the end of the 100 m segment (100). The side of the road measured is denoted by color.

capacity than the right side. For Road 2, the left and right sides had similar capacities on average, though there appeared to be some variation in which side had a higher capacity at a given time. The center consistently had a lower capacity, except for a measurement event at the end of the segment in late April 2022, when the capacities were high throughout the road. This was due to the ground still being frozen at that time.

For Road 1, the bearing capacity was on average 28 MPa (SD 11 MPa, range 9–60 MPa) on the left side and 29 MPa (SD 11 MPa, range 10–57 MPa) on the right side. For Road 2 the averages were 22 MPa (SD 13 MPa, range 4–66 MPa) for the center, 36 MPa (SD 15 MPa, range 10–90 MPa) for the left side, and 33 MPa (SD 17 MPa, range 9–85 MPa) for the right side. Overall, the bearing capacity was highest on measurement days when the road surface was slightly frozen in spring and autumn but reduced to only 10–20% of this value during the worst periods in spring and autumn. The time series of the bearing capacity appears to roughly follow the temperature curves presented in Figure 3.

Between road segments, the variation in road moisture content and bearing capacity was relatively large when measurements were taken on the day of the wet spring thaw and the day of the dry summer period (Figure 5). On the days of the dry summer and the spring thaw, the averages of the bearing capacity were 41 MPa (SD 15, range 21–90 MPa) and 24 MPa (SD 12 MPa, range 8–54 MPa), and the moisture content of the road was 11% (SD 7%, range 4–36%) and 19% (SD 10%, range 5–39%), respectively. On average, the bearing capacity was 51% lower during the day of spring thaw than during the dry summer, while the moisture of the road structure was 171% higher. There seems to be a tendency for soil coarseness to affect measured bearing capacity and VWC. The finer the road structure and/or subsoil, the lower the bearing capacity and the higher the VWC.

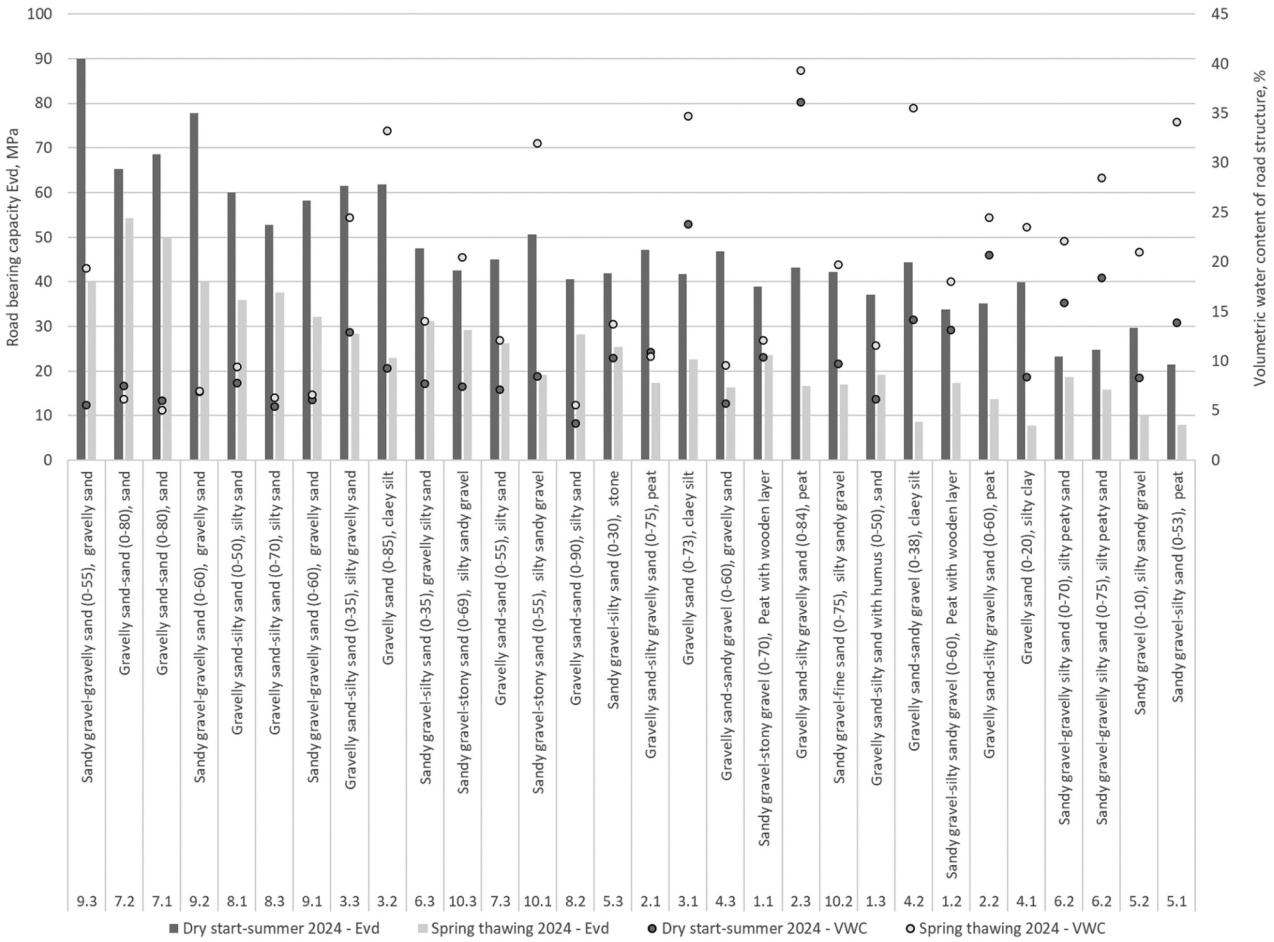


**Figure 5.** Measured bearing capacity and soil moisture of the road on spring thaw (15 May 2024) and dry summer (19 June 2024) days at each of the road segment sensor locations (30 in total). For each road segment (segment numbers are shown in the x-axis labels), the soil types and the thickness of the road structure (presented in cm), are shown. The moisture values in the VWC were the average of two moisture sensors located at 20 and 50 cm depth on the road structure. The road segments were ranked from highest to lowest according to the average bearing capacity of each segment.

### *Stress test for road 2*

The stress test on Road 2 revealed no major rutting, even after 30 passes. The maximum observed rut depth on road 2 was 2.5 cm after 30 passes (Figure 6). Negative rut depths can be explained by the extrusion of the road surface next to the wheel path, resulting from the truck wheel path not coinciding with the predetermined measurement points. The main increase in depth in rutting occurred in the first 10 passes, with continued rutting slowing down up to 30 passes. The first 10 passes resulted in average 1.3 cm depth ruts, whereas the last 10 passes only added 0.6 cm.

Before the truck tests on 17 May 2022, bearing capacities were measured with a LFWD, and the mean value of measurements from wheel paths on Road 2 was 25.2 MPa resulting in the second lowest mean bearing value of the one-year measurement period. The ambient temperature during the tests was 7.4°C and road temperatures from three road locations ranged from 0.3–8.3°C, 6.1–8.3°C, and 5.3–6.0°C at road depths of 20, 50 and 80 cm, respectively. The VWC values at the respective locations and depths ranged from 16–38%, 31–43%, and 36–43%. On Road 2, peat depths at the roadside were 230 cm at 20 m, over 250 cm at 40–80 m, and 204 cm at 100 m.

The pressure measurement unit detected all truck axle wheel passes at valid distances when analyzing the pressure variation of the sensor values at depths of 0.25 m and 0.4 m (Figure 7). However, the pressure peak values did not correspond to the weight distribution on the axles of the tested timber truck. This clearly indicated that the measuring frequency of the Bolling probe setup (15 Hz) was far too low for the vehicle speed of 15 km/h in the road tests. Due to the sparseness of the data, it was not possible to reliably determine the maximum pressure values induced by the vehicle wheels from a single pass.

### *Traffic monitoring with AI-based machine vision*

The classification results based on the limited sample of game camera photos proved to be surprisingly good. The ResNet50 CNN's training performance converged quickly within 200–300 epochs to around 93% overall accuracy on the validation photo set. The overall accuracy was over 97% for the test photo set, and the class-wise accuracies were all high, with the exception of Class 3 (Tractor) where the accuracy was 67%, reflecting the very limited number of tractors in the training

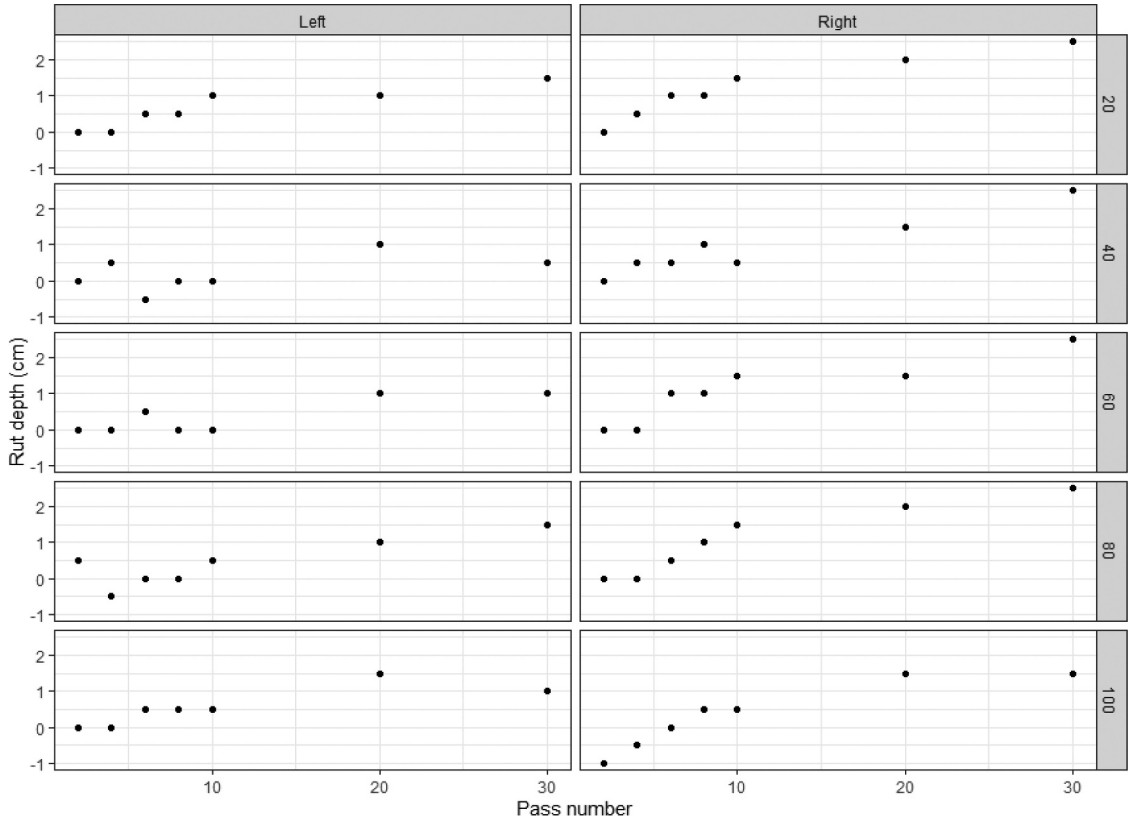


**Figure 6.** Rut depths on road 2 by wheel path, measurement location and number of passes. The measurement locations are shown in the caption on the right as meters along the road segment. Negative rut depth indicates uplift of road surface. A loaded 4-axle timber truck with a total weight of 39,360 kg was used in the stress tests for a total of 30 passes.

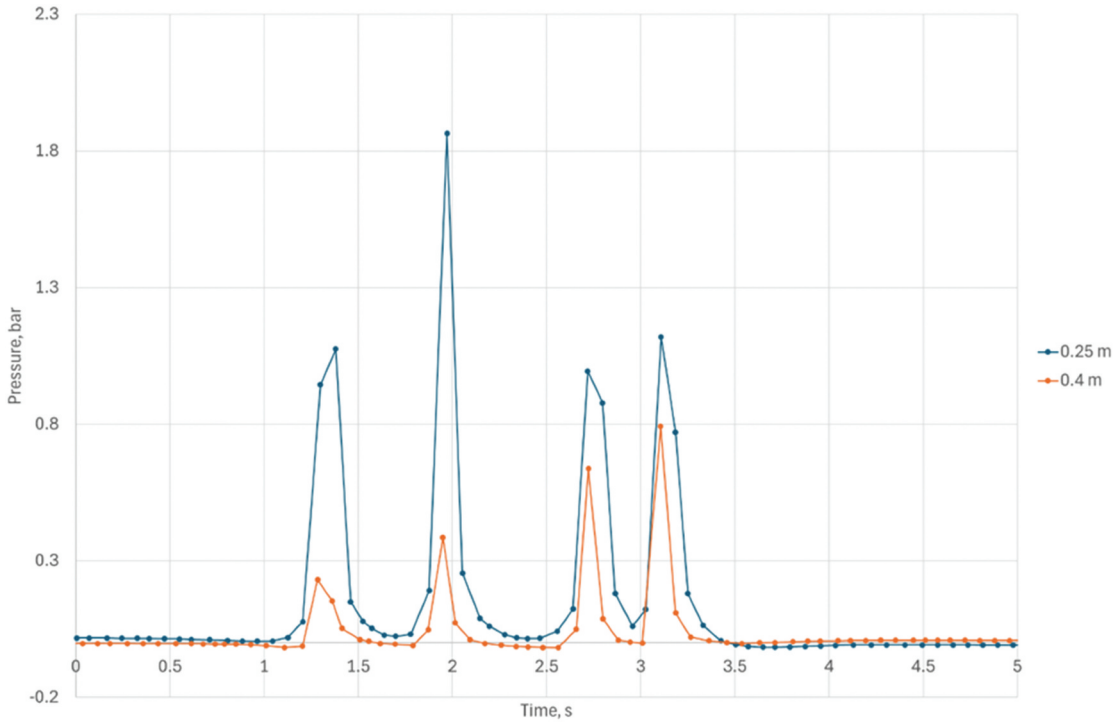


**Figure 7.** Example of soil pressure measurements under the left wheel path at 60 m location on road 2 at depths of 0.25 m and 0.4 m using the Bolling probe measuring equipment. The third sensor hose at a depth of 0.6 m was damaged during installation. A loaded four-axle timber truck weighing 39,360 kg was used in the stress test.

**Table 4.** The confusion matrix of the machine-learning-based classification accuracy of game-camera images for the test photos.

| | Predicted classes | | | |
|---|---|---|---|---|
| Actual classes | Cars and vans | Other | Heavy vehicle | Tractor |
| Cars and vans | 46 | 1 | 0 | 0 |
| Other | 0 | 37 | 0 | 0 |
| Heavy vehicle | 0 | 0 | 12 | 0 |
| Tractor | 0 | 0 | 2 | 4 |
| Producer's accuracy | 97.9% | 100.0% | 100.0% | 66.7% |
| User's accuracy | 100.0% | 97.4% | 85.7% | 100.0% |
| Overall accuracy | | 97.1% | | |

data (Table 4). The two misclassified tractor images were erroneously classified as heavy traffic, and one car/van was erroneously classified as "Other," while all the "Other" images were correctly classified. The high user's accuracies of the model suggests that when the CNN predicts a specific class, it is most frequently the correct one.

## Discussion

In this paper, a comprehensive system for monitoring variables contributing to the trafficability of forest roads in Finland was presented. Such long-term, hourly road weather monitoring at this scale has not previously been undertaken for forest roads. By the beginning of 2025, the first established road stations will have been in operation for almost three and a half years. Closely comparable settings with a smaller number of road sections and/or shorter follow-up periods have been reported, for example, by Holzleitner et al. (2020) on forest roads, and Saarenketo and Aho (2005) on low-volume gravel roads and Niskanen et al. (2024) on public gravel roads.

The variation of VWC and bearing capacity between and within road segments was found to be high on the same day of data collection under comparable weather conditions. The results add to the knowledge of the large temporal and spatial variation in the bearing capacity/trafficability of forest roads (e.g. Saarenketo and Aho 2005; Kaakkurivaara et al. 2015; Karjalainen et al. 2024). Of the 10 road sections, it was found that the coarser the road structure and subgrade, or the lower the soil moisture, the higher the modulus of elasticity of the road. This agrees well with the findings of Fjeld et al. (2023).

When the bearing capacity of forest roads was monitored with the same type of LFWD instrument, the mean and range of E-modulus values measured by Holzleitner et al. (2020), Fjeld et al. (2023) and Karjalainen et al. (2024) were highly comparable to the corresponding values in our study. Using a different type of LFWD device (Loadman), the E-modulus values obtained from low-volume forest roads were higher than in our study (Kaakkurivaara et al. 2015).

Closer analysis of the two road segments (1 and 2) showed that the sensors are reliable, with no missing data from the weather station, and only two missed hourly recordings from one of the sensor systems during the one-year test run. Throughout the study, the temperature measurements were credible when visually compared with weather data from the Finnish Meteorological Institute (FMI), but the total rainfall was unrealistic. This was significantly higher than the approximately 600 mm of rainfall measured by established weather stations nearby, even though this includes the snowfall from winter months measured as the equivalent amount of liquid water. However, the peaks in rainfall did correspond to increases in soil moisture, so the data could still be a valuable though imperfect source of local weather conditions. One possible reason for recorded higher rainfall during rainy periods was the presence of tall forest close to the weather station. This can allow additional water droplets to fall from the canopy onto the sensor even after the rain has stopped.

In addition, the soil moisture sensor has been validated in a laboratory environment for VWC monitoring, demonstrating high accuracy. It should be noted, however, that the soil moisture sensor used is unable to provide valid moisture content values in conditions where the ground is frozen. In other words, the sensor monitors liquid water content by volume, meaning that VWC sensor data can only be used for modeling purposes during non-frozen periods.

The bearing capacity of the roads correlated well with temperatures and soil moisture, so weather data could potentially be used to predict changes in bearing capacity. To build and validate such models, data from all 10 road sections with longer follow-up are needed. In addition, satellite data from the Soil Moisture Active and Passive Mission (SMAP) with soil moisture estimates at different depths have recently confirmed good predictive power for the bearing capacity of forest roads (Fjeld et al. 2023) and rutting on forest soils (Schönauer et al. 2024).

On the two test roads with 1 year of follow-up, the highest bearing capacities were measured when the road surface was slightly frozen. This occurred during a sequence of cold days below zero in late autumn (measured on 10 November 2021) and during the frost-thaw spring season after a cold night (22 April 2022). However, during the most volatile periods in spring and autumn, the bearing capacities were only 10–20% of the highest values measured. Additionally, dry summer conditions positively affected the bearing capacity.

The change in bearing capacity can be rapid and noticeable even within a single day, as demonstrated by two sets of measurements on Road 2 on 22 April 2022. After a cold night, the frost on the road began to melt as the day progressed, causing the bearing capacity of the daytime recordings to drop to an average of 45% of the early morning values. Under such thaw and wet road conditions, there is a high risk of heavy traffic causing severe damage to the road structure, potentially halting the use of the road until the road has recovered.

During the stress tests, no major rutting was observed on Road 2, even though the segments were traversed up to 30 times by a heavy timber truck. This was unexpected because Road 2 was built on a peatland, and the tests were conducted in late spring when the VWC in the road structure was high (ranging from 16–43%). Possible explanations for the limited rutting include the thick and stiff wearing and base course and subbase layers, the high-quality road structure material used, and the brushwood mattress between peat (subgrade) and the subbase layers. Peaty subsoil with such road construction acts like a trampoline, bending under the load stress but returning after the truck passes. In addition, the roadside embankments/shoulders were flattened to a shallower gradient, resulting in a wider embankment than usually, in order to spread the load over the wider foundation (see e.g. Munro 2004). Furthermore, the E-modulus values recorded by the LFWD tend to be lower on peaty subsoils than on mineral subsoils due to the greater deflection of the road under the loading plate. For modeling road trafficability, more data from stress tests with heavy vehicles on different subsoil types and road structures under various weather conditions are needed.

The pressure sensor measurement results during the stress tests indicate that a sampling frequency of at least 1 kHz or higher is necessary to capture the pressure maxima created by traffic (see e.g. Lamandé and Schjønning 2011). Therefore, the measurement system used in this study has been rebuilt based on analogue pressure transducers and a datalogger. With the revised setup, the measurement frequency is limited by the datalogger, eliminating the time lost in two-way communication between the laptop and pressure sensors. The maximum sampling rate is now 200 kHz. Equipment with much lower recording frequencies is likely to miss the maximum pressure applied by passing traffic, which is crucial for estimating the impact of traffic on road conditions.

The classification of traffic from game camera photographs based on convolutional neural networks performed very well, with only about 2% cars/vans misclassified as "Other," while a third of the six tractor pictures were misclassified as "Heavy traffic," with all "Other"-pictures correctly classified. A comparable classification accuracy of 95% was achieved by Bautista et al. (2016) when using CNN to detect and classify vehicles in low-resolution videos. Although the classification results are good, it is important to note that the test dataset is limited in size. This issue could be addressed in the future by acquiring more data or employing techniques like nested cross-validation to enhance the reliability of performance estimation. Overall, given the good performance on the test dataset, it is reasonable to expect that a CNN-based computer vision approach will perform well in automatic vehicle classification in a production environment, especially with more data available. Thus, our results indicate that the use of game cameras could provide reliable traffic detection in a cost-effective manner and link the effects of heavy traffic and road maintenance on road quality and trafficability (i.e. surface deformation).

The results show that air temperature and precipitation are highly correlated with road temperature and moisture, and that the relationship between these road weather parameters and road bearing capacity is clear. Therefore, it would be useful to build accurate models that relate soil temperature and moisture to air temperature and precipitation for dynamic trafficability monitoring. Building and validating such models requires more data, but this could be done with a limited number of roads as long as the observation period is long enough to include year to year variations with a sufficient number of observations of the bearing capacity from both low and high ends. Furthermore, by improving the measurements, such as including frost monitoring, more detailed predictions of spring thaw weakening and frost melting on the road could be modeled (e.g. Saarenketo and Aho 2005; Niskanen et al. 2024). In addition, based on our soil samples, the soil type map provided by the Geological Survey of Finland was promising in providing semi-precise spatial data for our road sections. First pilot area tests have shown that 1:20 000 soil maps with improved accuracy could be produced for the whole of Finland (Middleton and Kanaoja 2023).

Assessing the static condition of a road could help predicting its trafficability. Airborne Laser Scanning (ALS) data, with a density of 5 pts/m2 have been successfully used for assessing road condition characteristics, such as road width and ditch depth (e.g. Karjalainen et al. 2024, 2024). In addition, satellite SMAP data, wetness maps and DEM information should be considered in model development (e.g. Schönauer et al. 2022; Fjeld et al. 2023). Combining these data with automatically monitored sensor data from forest roads would enable a more detailed analysis of road quality and trafficability changes, as well as the prediction of the road's dynamic bearing capacity.

This paper suggests that long-term continuous monitoring of road weather, supplemented by static information on road structure and materials and measurements of forest road bearing capacity, provides the basis for a digital twin of forest roads. Road stress testing and automated monitoring of traffic and road maintenance will further improve understanding of the behavior of weather-road-vehicle interactions and the impact of heavy traffic on forest roads. These elements and steps align well with the main components presented by Chen et al. (2022) for predicting road performance and condition using a digital twin.

In a recently completed project, the first version of the Forest Road Hub, which graphically displays road weather data and the bearing capacities from the road weather stations presented in this paper, has been made available online. The Forest Road Hub is a framework concept for presenting the digital twin of a forest road (Luke 2024). It illustrates the temporal variation of the road weather characteristics and the modulus of elasticity of the road, providing a visual interpretation of the interactions between the displayed variables and the weather parameters that affect the road's bearing capacity. The digital twin framework will be further developed by including other elements and parameters that affect the bearing capacity of forest road.

## Conclusions

In this work, the feasibility of monitoring several key components to pave the way for the digital twin of forest roads was demonstrated. It was shown that weather conditions of forest roads can be reliably monitored using sensors embedded in the

road, as well as on-site weather stations. By linking road bearing capacity to road weather data, the dynamic trafficability of forest roads can be modeled. Methods for monitoring heavy traffic using both pressure sensors and game camera images combined with AI-based vehicle type classification were also demonstrated.

Most importantly, it was shown that the bearing capacity of forest roads during the most critical periods can be only 10–20% of their maximum value, highlighting the need for reliable real-time solutions to inform road users about the condition and trafficability of forest roads. Using the approach presented, a digital twin can be developed in the future to not only monitor but also predict the dynamic trafficability of forest roads.

## Disclosure statement

No potential conflict of interest was reported by the author(s).

## Funding

This study was part of the Secure Log project funded by Luonnonvarakeskus (Luke) and the regionally funded project "Take Me Home Country Road," supported by the European Union's regional and structural funds. These projects laid the foundation for automated online monitoring of road weather data and the establishment of road stations. The paper was finalized with the funding from the Academy of Finland Flagship Programme (Forest-Human-Machine Interplay (UNITE)) grant No [337653]; Research Council of Finland.

## References

Abadi M, Agarwal A, Barham P, Brevdo E, Chen Z, Citro C, Corrado GS, Davis A, Dean J, Devin M, et al. 2016. TensorFlow: large-scale machine learning on heterogeneous distributed systems. arXiv. doi: 10.48550/arXiv.1603.04467.

Alzubaidi H, Magnusson R. 2002. Deterioration and rating of gravel roads: state of the art. Road Mater Pavement Des. 3(3):235–260. doi: 10.1080/14680629.2002.9689924.

Bautista CM, Dy CA, Mañalac MI, Orbe RA, Cordel M. 2016. Convolutional neural network for vehicle detection in low resolution traffic videos. 2016 IEEE Region 10 Symposium (TENSYMP); 9-11 May; Bali, Indonesia; 277–281.

Boschert S, Rosen R. 2016. Digital twin—the simulation aspect. In: Hehenberger P Bradley D, editors. Mechatronic futures, challenges and solutions for mechatronic systems and their designers. Cham: Springer; p. 59–74.

Chen K, Eskandari Torbaghan M, Chu M, Zhang L, Garcia-Hernández A. 2022. Identifying the most suitable machine learning approach for a road digital twin. Proc Inst Civ Eng - Smart Infrastructure And Construction. 174(3):88–101. doi: 10.1680/jsmic.22.00003.

Chollet F. 2015. Keras. [accessed 2024 Sep 18]. https://github.com/fchollet/keras.

Consilvio A, Hernández JS, Chen W, Brilakis I, Bartoccini L, Di Gennaro F, Van Welie M. 2023. Towards a digital twin-based intelligent decision support for road maintenance. Transportation Research Procedia. 69:791–798. doi: 10.1016/j.trpro.2023.02.237.

Deng J, Dong W, Socher R, Li L-J, Li K, Fei-Fei L. 2009. ImageNet: a large-scale hierarchical image database. 2009 IEEE Conference on Computer Vision and Pattern Recognition; 20-25 June; Miami, (FL), USA; 248–255.

Digital Twin Consortium. 2025. Definition of a digital twin. [accessed 2025 Jan 6]. https://www.digitaltwinconsortium.org/initiatives/the-definition-of-a-digital-twin/.

FinLex. 2013. Valtioneuvoston asetus ajoneuvojen käytöstä tiellä annetun asetuksen muuttamisesta [Government Degree about changing the regulation on the use of vehicles on the road]. [accessed 2025 Jan 7]. https://www.finlex.fi/fi/laki/alkup/2013/20130407.

Fjeld D, Bjerketvedt J, Bråthen M. 2022. Bæreevneklassifisering for skogsbilveier-Resultater av pilotforsøket 2018-2021 [Bearing capacity classification for forest roads-Results of pilot study 2018-2021]. Nibio Rapport no: 8/147/2022.

Fjeld D, Persson M, Fransson JES, Bjerketvedt J, Bråthen M. 2023. Modelling forest road trafficability with satellite-based soil moisture variables. Int J For Eng. 35(1):93–104. doi: 10.1080/14942119.2023.2276628.

Greis I, Perälä M, Perälä T, Teppo M. 2019. Metsänhoidon suositukset metsäteiden kunnossapitoon, työopas [Forest management recommendations for forest road maintenance, workbook]. Helsinki: Tapion julkaisuja, Tapio Oy.

GTK. 2018. Superficial deposits 1: 20 000/1: 50 000. [accessed 2021 Nov 5]. https://tupa.gtk.fi/paikkatieto/meta/maapera_20_50k.html.

He K, Zhang X, Ren S, Sun J. 2016. Deep residual learning for image Recognition. 2016 IEEE Conference on Computer Vision and Pattern Recognition (CVPR), In 2016 IEEE Conference on Computer Vision and Pattern Recognition (CVPR); 27-30 June; Las Vegas, (NV), USA; 770–778.

Holzleitner F, Fritz M, Sokol W, Zott F, Kanzian C. 2020 Sep 22–24. Predicting forest road´s bearing capacity using smart sensing technology. In: Björnheden R Callesen I editors. NB Nord2020. Proceedings of the Forest Operations For The Future; Denmark: Helsinore. p. 27–32.

Hämäläinen E. 2012. Yksityisteiden kunnossapito. Kunnossapitotöiden suunnittelun ja toteuttamisen perusteet [Maintenance of private roads. Basics of planning and execution of maintenance works]. Kerava: Suomen tieyhdistys.

Jiang F, Ma L, Broyd T, Chen W, Luo H. 2022. Digital twin enabled sustainable urban road planning. Sustain Cities Soc. 78:103645. doi: 10.1016/j.scs.2021.103645.

Jones D, Snider C, Nassehi A, Yon J, Hicks B. 2020. Characterising the digital twin: a systematic literature review. CIRP J Manuf Sci Technol. 29(A):36–52. doi: 10.1016/j.cirpj.2020.02.002.

Kaakkurivaara T. 2018. Innovative methods for measuring and improving the bearing capacity of forest roads [dissertationes Forestales 251]. University of Helsinki.

Kaakkurivaara T, Korpunen H. 2017. Increased fly ash utilization — value addition through forest road reconstruction. Can J Civ Eng. 44(3):223–231. doi: 10.1139/cjce-2016-0193.

Kaakkurivaara T, Vuorimies N, Kolisoja P, Uusitalo J. 2015. Applicability of portable tools in assessing the bearing capacity of forest roads. Silva Fenn. 49(2):1239. doi: 10.14214/sf.1239.

Karjalainen T, Karjalainen V, Waga K, Tokola T. 2024. Predicting the roadway width of forest roads by means of airborne laser scanning. Int J Appl Earth Observ Geoinf. 133:104109. doi: 10.1016/j.jag.2024.104109.

Karjalainen V, Jukka Malinen J, Tokola T. 2024. Predicting bearing capacity and trafficability classes of forest roads using road properties and surrounding terrain information. Road Mater Pavement Des. 1–18. doi: 10.1080/14680629.2024.2434945.

Keller T, Ruiz S, Stettler M, Berli M. 2016. Determining soil stress beneath a tire: measurements and simulations. Soil Sci Soc Am J. 80(3):541–553. doi: 10.2136/sssaj2015.07.0252.

Kim N, Lee J-S, Park G, Kang S, Han W, Hong W-T. 2023. Strength and stiffness characterizations of geo-materials composing unpaved roads using LFWD, DCP, and CDP tests. Constr Build Mater. 402:132592. doi: 10.1016/j.conbuildmat.2023.132592.

Kingma DP, Ba J. 2015. Adam: a Method for stochastic optimization. Proceedings of the International Conference on Learning Representations (ICLR); San Diego, (CA), USA.

Kulju I, Niinistö T, Peltola A, Räty M, Sauvula-Seppälä T, Torvelainen J, Uotila E, Vaahtera E. 2023. Metsätilastollinen vuosikirja 2022 Finnish statistical yearbook of forestry 2022. Helsinki, Finland, Luonnonvarakeskus.

Lamandé M, Schjønning P. 2011. Transmission of vertical stress in a real soil profile. Part II: effect of tyre size, inflation pressure and wheel load. Soil Tillage Res. 114(2):71–77. doi: 10.1016/j.still.2010.08.011.

Lehtonen I, Venäläinen A, Kämäräinen M, Asikainen A, Laitila J, Anttila P, Peltola H. 2019. Projected decrease in wintertime bearing capacity on different forest and soil types in Finland under a warming climate. Hydrol Earth System Sci. 23(3):1611–1631. doi: 10.5194/hess-23-1611-2019.

Liu M, Fang S, Dong H, Xu C. 2021. Review of digital twin about concepts, technologies, and industrial applications. J Manuf Syst. 58(B):346–361. doi: 10.1016/j.jmsy.2020.06.017.

Luke. 2024. Luke – Metsätiehub [Luke – Forest Road Hub]. [accessed 2024 Dec 16]. https://countryroads.luke.fi/dashboard.

Machl T, Donaubauer A, Kolbe TH. 2019. Planning agricultural core road networks based on a digital twin of the cultivated landscape. J Digit Landsc Archit. 316–327.

Metsätieohjeisto. 2001. Guidelines for forest roads. Helsinki: Metsäteho Oy.

Meža S, Pranjić MA, Vezočnik R, Osmokrović I, Lenart S, Biancardo SA. 2021. Digital twins and road construction using secondary raw materials. J Adv Transp. 2021:1–12. doi: 10.1155/2021/8833058.

Middleton M, Kanaoja T. 2023. Maaperäpilotti. Geologian Tutkimuskeskus GTK. [accessed 2025 Jan 8]. https://mmm.fi/documents/1410837/188518233/12+Maaper%C3%A4pilotti+Middleton.pdf/48c55ad5-cd8c-a94f-9576-a9b5c3ffe5a9/12+Maaper%C3%A4pilotti+Middleton.pdf?t=1699902242535.

Munro R. 2004. Dealing with bearing capacity problems on low volume roads constructed on peat. Including case histories from roads projects within the ROADEX partner districts. Roadex II. Northern Periphery; [accessed 2025 Jan 8]. https://www.roadex.org/wp-content/uploads/2014/01/2_5-Roads-on-Peat_l.pdf.

Niskanen P, Pirnes V, Pekkala V, Rasi-Koskinen H, Tuutijärvi M-T, Jokinen K, Sukuvaara T, Karsisto V, Mäenpää K. 2024. Winter Premium. Raportti n:o 13. Mechanical engineering, University of Oulu, Oulu; [accessed 2025 Jan 8]. https://urn.fi/URN:NBN:fi:oulu-202403152264.

Pidwerbesky B. 1997a. Predicting rutting in unbound granular base-courses from Loadman and other in-situ non-destructive tests. Road Transp Res. 6(3):16–25.

Pidwerbesky B. 1997b. Evaluation of non-destructive in-situ tests for unbound granular pavements. IPENZ Trans. 24(1):12–17.

Roadscanners. 2025. Roadscanners' Spring thaw services. [accessed 2025 Jan 15]. https://www.roadscanners.com/services/spring-thaw-services/.

Ruosteenoja K, Jylhä K. 2021. Projected climate change in Finland during the 21st century calculated from CMIP6 model simulations. Geophysica. 56(1):39–69.

Saarenketo T, Aho S. 2005. Managing spring thaw weakening on low volume roads. Problem description, load restriction policies, monitoring and rehabilitation. Roadscanners Roadex II Northern Periphery.

Schönauer M, Prinz R, Väätäinen K, Astrup R, Pszenny D, Lindeman H, Jaeger D. 2022. Spatio-temporal prediction of soil moisture using soil maps, topographic indices and SMAP retrievals. Int J Appl Earth Observ Geoinf. 108:102730. doi: 10.1016/j.jag.2022.102730.

Schönauer M, Ågren AM, Katzensteiner K, Hartsch F, Arp P, Drollinger S, Jaeger D. 2024. Soil moisture modeling with ERA5-land retrievals, topographic indices, and in situ measurements and its use for predicting ruts. Hydrol Earth Syst Sci. 28(12):2617–2633. doi: 10.5194/hess-28-2617-2024.

SFS-EN 932-1. 2003. Kiviainesten yleisten ominaisuuksien testaus. Osa 1: Näytteenottomenetelmät. [Tests for general properties of aggregates. Part 1: methods for sampling.]. 27 Helsinki: Suomen standardisoimisliitto.

SFS-EN 933-1. 2013. Kiviainesten geometristen ominaisuuksien testaus. Osa 1: Rakeisuuden määrittäminen. Seulontamenetelmä. [Tests for geometrical properties of aggregates. Part 1: Determination of particle size distribution. Sieving method.]. 19 Helsinki: Suomen standardisoimisliitto.

SFS-EN 1097-5. 2010. Kiviainesten mekaanisten ja fysikaalisten ominaisuuksien testaus. Osa 5: Kosteuspitoisuuden määrittäminen kuivaamalla tuuletetussa lämpökaapissa. [Tests for mechanical and physical properties of aggregates. Part 5: determination of the water content by drying in a ventilated oven.]. 12 Helsinki: Suomen standardisoimisliitto.

Solonen H, Väätäinen K, Tokola T, Kärhä K. 2023. Metsäautotienkäyttäjien hiljainen tieto: Haastattelututkimus puutavara-autokuljetusyrittäjille ja kuljettajille [Tacit knowledge of forest road users: an interview based survey of timber transport entrepreneurs and truck drivers]. Luonnonvara- ja biotalouden tutkimus 116/2023. Helsinki, Luonnonvarakeskus.

Solonen H, Väätäinen K, Tokola T, Venäläinen P, Anttila P, Kärhä K. 2024. Metsäteiden kuljetuskelpoisuustiedon visio ja tiekartta : Alemman tieverkon liikennöitävyys ja ympärivuotisen puuhuollon turvaaminen [Trafficability of the low volume road network and securing the year-round supply of wood]. Luonnonvara- ja biotalouden tutkimus 43/2024. Helsinki, Luonnonvarakeskus.

Steyn W, Broekman A. 2022. Development of a digital twin of a local road network: a case study. J Test Eval. 50(6):2901–2915. doi: 10.1520/JTE20210043.

Strandström M. 2017. Päällysrakenneluokat – Metsätieohjeiston uudistettu materiaali 2017 [Superstructure classes - Revised Forest Road Guide 2017]. Metsäteho Oy; [accessed 2024 Oct 24]. https://www.metsateho.fi/wp-content/uploads/P%C3%A4%C3%A4llysrakenneluokat.pdf.

Söhne W. 1958. Fundamentals of pressure distribution and soil compaction under tractor tires. Agric Eng. 39:290.

Test Method Q258A. 2021. Test Method Q258A: dynamic modulus of deformation – light falling weight device – accelerometer type. Materials testing manual – part 5, transport and main roads. [accessed 2024 Oct 2]. https://insitutek.com/wp-content/uploads/2022/06/Test-Method-Q258A-Dynamic-Modulus-of-Deformation-Light-Falling-Weight-Device-Accelerometer-Type-Department-of-Transport-and-Main-Roads-Queensland-DTMR-March-2021.pdf.

Truebner SMT100. 2024. Soil moisture sensor SMT100. Manual. 10 p. https://www.truebner.de/assets/download/Manual_SMT100_V1.0.pdf.

Vuorimies N, Kolisoja P, Kaakkurivaara T, Uusitalo J. 2015. Estimation of the risk of rutting on forest roads during the spring thaw. Transp Res Rec. 2474(1):143–148. doi: 10.3141/2474-17.

ZFG. 2024. ZFG 3.1 - light weight deflectometer (LWD). Zorn instruments GmbH & Co. KG. 2. [accessed 2025 Jan 7]. https://www.zorn-instruments.com/fileadmin/redaktion/zorn_instruments_de/infocenter/downloads/Fallgewichtsger%C3%A4te/202401_Flyer_ZFG_3.1_A4_2seitig_Eng_web.pdf.